Sensing relative signal in the Tgf-β/Smad pathway

Christopher L. Frick[a,1], Clare Yarka[a], Harry Nunns[a], and Lea Goentoro[a,1]

[a]Division of Biology and Biological Engineering, California Institute of Technology, Pasadena, CA 91125

Edited by Arup K. Chakraborty, Massachusetts Institute of Technology, Cambridge, MA, and approved February 3, 2017 (received for review July 12, 2016)

How signaling pathways function reliably despite cellular variation remains a question in many systems. In the transforming growth factor-β (Tgf-β) pathway, exposure to ligand stimulates nuclear localization of Smad proteins, which then regulate target gene expression. Examining Smad3 dynamics in live reporter cells, we found evidence for fold-change detection. Although the level of nuclear Smad3 varied across cells, the fold change in the level of nuclear Smad3 was a more precise outcome of ligand stimulation. The precision of the fold-change response was observed throughout the signaling duration and across Tgf-β doses, and significantly increased the information transduction capacity of the pathway. Using single-molecule FISH, we further observed that expression of Smad3 target genes (*ctgf*, *snai1*, and *wnt9a*) correlated more strongly with the fold change, rather than the level, of nuclear Smad3. These findings suggest that some target genes sense Smad3 level relative to background, as a strategy for coping with cellular noise.

signal transduction | fold-change detection | Tgf-β | Smad | information

Variability in the abundance of signaling components, across cells and contexts, is a well-documented feature of multiple signaling pathways (1–3). Several ideas have been proposed for how cells can overcome variability: Cells may integrate responses from multiple signaling pathways (1), compensate via cross-talk with other pathways (4), average responses across neighboring cells (1), use negative feedbacks (5), or measure signal dynamics (6). In our own work, we found another strategy, where cells overcome variability by interpreting signaling relative to background (7). Specifically, working in the canonical Wnt pathway, we presented evidence that signal is transduced through the ligand-induced fold change in β-catenin level, rather than the absolute level.

Detecting fold change in signal level allows a cell to assign meaning to signal relative to its own background, enabling faithful transduction despite cellular variability. In addition to the Wnt pathway, fold-change detection has been proposed in the Erk pathway (2) and, subsequently, in the NF-κB pathway (3), calcium signaling (8), and cytokine signaling (9). The evidence for fold-change detection in more and more systems suggests a conserved strategy across signaling pathways in animal cells. Motivated by these findings, we explored in this study for the presence of fold-change detection in a major channel of communication in cells, the transforming growth factor-β (Tgf-β) pathway.

The Tgf-β pathway functions across diverse contexts and tissues, and regulates fundamental processes, including proliferation, differentiation, morphogenesis, stem-cell maintenance, and regeneration (10). These diverse functions are mediated by a highly conserved set of proteins. The Tgf-β pathway senses signal from a large family of secreted ligands, whose members include Tgf-β, Bmp, and Activin. Signal transduction is primarily mediated by the Smad proteins (Fig. 1*A*): five ligand-specific receptor Smads (R-Smads; Smad1, Smad2, Smad3, Smad5, and Smad8), one common Smad (Smad4), and two regulatory Smads (Smad6 and Smad7) that act as feedback. The Smad proteins transduce signal in a dynamic process: They continually shuttle between the cytoplasm and nucleus, and ligand stimulation tunes this process. Specifically, ligand binds a complex of type I and type II serine/threonine kinase receptors, which phosphorylate the R-Smads. Phosphorylated R-Smads form a complex with the common Smad4. In their heteromeric form, the Smad proteins are retained more strongly in the nucleus through reduced export rate, as well as, as proposed recently (11), accelerated import rate. Thus, ligand activation leads to a net accumulation of the Smad complex in the nucleus, where it regulates target genes.

The Tgf-β pathway is a particularly interesting system for testing for fold-change detection because it is known that the expression levels of its components vary considerably from cell to cell. A recent study using proximity ligation assay in fixed cells revealed that the levels of Smad3/4 and Smad2/4 complexes vary by more than 40-fold across cells (12). Consistent with this finding, our immunofluorescence analysis in a clonal cell population revealed significant overlap between the level of nuclear Smad3 in unstimulated and stimulated cells (Fig. S1). The variability in the level of Smad proteins from cell to cell raises the question as to how cells can reliably sense information about their external environment through the Tgf-β pathway.

Motivated by these observations, we tested whether signal in the Tgf-β pathway is sensed in an absolute manner or relative to background. Finding fold-change response in the Tgf-β pathway would expand our understanding of how information flows in the pathway, and how pathway activity should be interpreted appropriately across contexts and diseases. The alternative finding is equally interesting: If we find that cells monitor the absolute level of Smad proteins despite their variability, this finding will suggest that the mechanism that produces robust cellular outcomes is downstream from Smads.

Results

To investigate what aspects of Smad dynamics regulate gene response, we used live-cell imaging of the Tgf-β pathway. Responding to Tgf-β ligands, specifically, are the receptor-regulated Smad2 and Smad3 (R-Smads). Although structurally similar, Smad2 and Smad3 affect distinct genes (13), and it is also known that Smad3 can bind directly to DNA, whereas the predominant

Significance

It is not fully understood how cells process information in the face of noise. We posed this question in the transforming growth factor-β (Tgf-β) pathway, a major intercellular signaling pathway in animal cells. We found evidence that rather than sensing the signaling state of the Tgf-β pathway, cells sense the signaling state relative to background. Finding that signaling dynamics are interpreted in a relative manner may have implications for how we understand the pathway's context-dependent outcomes and roles in diseases. Our work reinforces an emerging principle that individual cells process signal in a relative manner.

Author contributions: C.L.F. and L.G. designed research; C.L.F. and C.Y. performed research; H.N. contributed new reagents/analytic tools; C.L.F. and C.Y. analyzed data; and C.L.F. and L.G. wrote the paper.

The authors declare no conflict of interest.

This article is a PNAS Direct Submission.

Freely available online through the PNAS open access option.

[1]To whom correspondence may be addressed. Email: goentoro@caltech.edu or cfrick@caltech.edu.

This article contains supporting information online at www.pnas.org/lookup/suppl/doi:10.1073/pnas.1611428114/-/DCSupplemental.

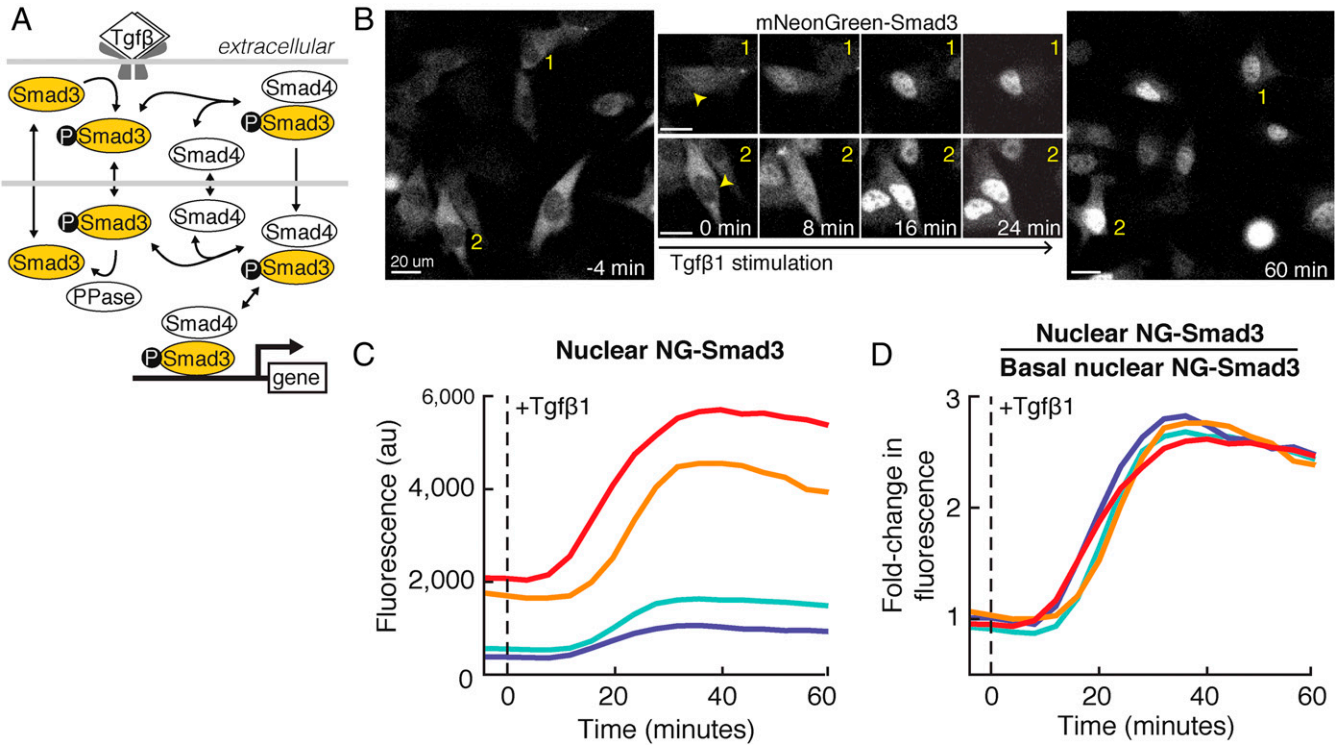

Fig. 1. Ligand-induced nuclear accumulation of NG-Smad3. (*A*) Illustration of Smad3 activation and nucleocytoplasmic shuttling in the Tgf-β pathway. Ligand stimulation leads to phosphorylation of Smad3. Phosphorylated Smad3 complexes with Smad4 are shown. The Smad complex translocates to the nucleus and regulates target genes. The Smad complex may also dissociate, allowing Smad3 dephosphorylation and export back to the cytoplasm. (*B*) NG-Smad3 in C2C12 clonal reporter cells responding to ligand stimulation. Purified Tgf-β1 (2.4 ng/mL) was added to the cells at the start of the experiment (denoted as t = 0 min). (*Left*) Cells are shown before stimulation. (*Center*) Two individual cells are tracked over time. (*Right*) Same cells 60 min after stimulation. (Scale bars: 20 μm.) (*C*) Quantitation of the level of nuclear NG-Smad3 during Tgf-β1 stimulation. Each line corresponds to an individual cell. The dashed line indicates when Tgf-β1 was added. au, arbitrary units. (*D*) Fold change in nuclear NG-Smad3 from the same cells measured in *C*. Basal level is measured as the average of the fluorescence level 24 min before ligand stimulation.

isoform of Smad2 does not (14). Here, we focused on Smad3 and generated a reporter C2C12 cell line stably expressing an mNeonGreen-Smad3 construct (NG-Smad3; the sequence is shown in Fig. S2*A*). Smad3 protein tagged on the N terminus retains phosphorylation at the C-terminal SXS motif, complex formation with Smad4, nuclear translocation, DNA binding, and transcriptional activity (15). We determined via Western blotting that NG-Smad3 is expressed at a moderate level, at twofold more than the endogenous Smad3 (Fig. S2 *B* and *C*). We confirmed that NG-Smad3 is phosphorylated (Fig. S2*D*) and translocates to the nucleus upon ligand stimulation (Fig. S2*E*). We further confirmed that the signaling response is quantitatively identical across three clonal lines (Fig. S3*B*). One clone was chosen for the measurements described here.

Stimulating the clonal reporter cells with Tgf-β ligand resulted in nuclear accumulation of NG-Smad3 (Fig. 1*B* and Movie S1), as expected from published studies (15–18). In this experiment, cells were stimulated with purified recombinant Tgf-β1 (2.4 ng/mL). Images were acquired every 4 min, starting at 1 h before to up to 4 h after ligand stimulation. We segmented the nucleus using fluorescence signal from constitutively expressed nuclear mCerulean3, and then quantified the median fluorescence of NG-Smad3 in the nucleus for each cell (*Materials and Methods*). Nuclear accumulation of NG-Smad3 began immediately upon Tgf-β1 addition and peaked in most cells after 30 min, consistent with previously reported time scales of R-Smad (15, 18). In nearly all cells, NG-Smad3 remained predominantly nuclear during the 4 h of imaging, with a slight decrease over time. We confirmed that cells only exposed to buffer showed no response (Fig. S4*A*).

Quantifying the NG-Smad3 response in single cells, we indeed observed that the level of nuclear NG-Smad3 varied across cells, even after Tgf-β1 stimulation (Fig. 1*C*). In fact, cells with a high initial level of nuclear NG-Smad3 responded more strongly to Tgf-β1 stimulation, arriving at a higher final level (e.g., the orange and red traces in Fig. 1*C*). In contrast, cells with a lower initial level of nuclear NG-Smad3, rather than compensating for the lower start, responded less to Tgf-β1 stimulation (e.g., the cyan and purple traces in Fig. 1*C*). Thus, the cells do not appear to adjust the strength of their response to produce a robust level of nuclear NG-Smad3.

In comparison, these same cells exhibited more precise fold-change responses. The fold-change responses can be seen in Fig. 1*D*, where we have now plotted the level of nuclear NG-Smad3 relative to the basal, prestimulus level. Indeed, the variability in Fig. 1*C* arises because exposure to ligand stimulates an increase in nuclear Smad3 proportional to the initial level (e.g., 200–600 and 2,000–6,000 are both threefold changes). The linear proportionality between the basal and stimulated levels of nuclear NG-Smad3 holds for nearly two orders of magnitude (Fig. S4*C*).

To confirm the higher precision in fold-change response, we quantified 299 cells responding to Tgf-β1 stimulation (Fig. 2). Across these cells, the level of nuclear NG-Smad3 varied from cell to cell (Fig. 2*A*; the distribution is shown in Fig. 2*C*). By contrast, the fold change in the level of nuclear NG-Smad3 is substantially more precise (Fig. 2*B*), resulting in a response distribution that is 3.7-fold more narrow than the absolute level distribution (computed using quartile coefficient of dispersion; Fig. 2*D*). These results are reproducible across experiments (Fig. S3*A*) and across three clonal cell lines (Fig. S3*B*).

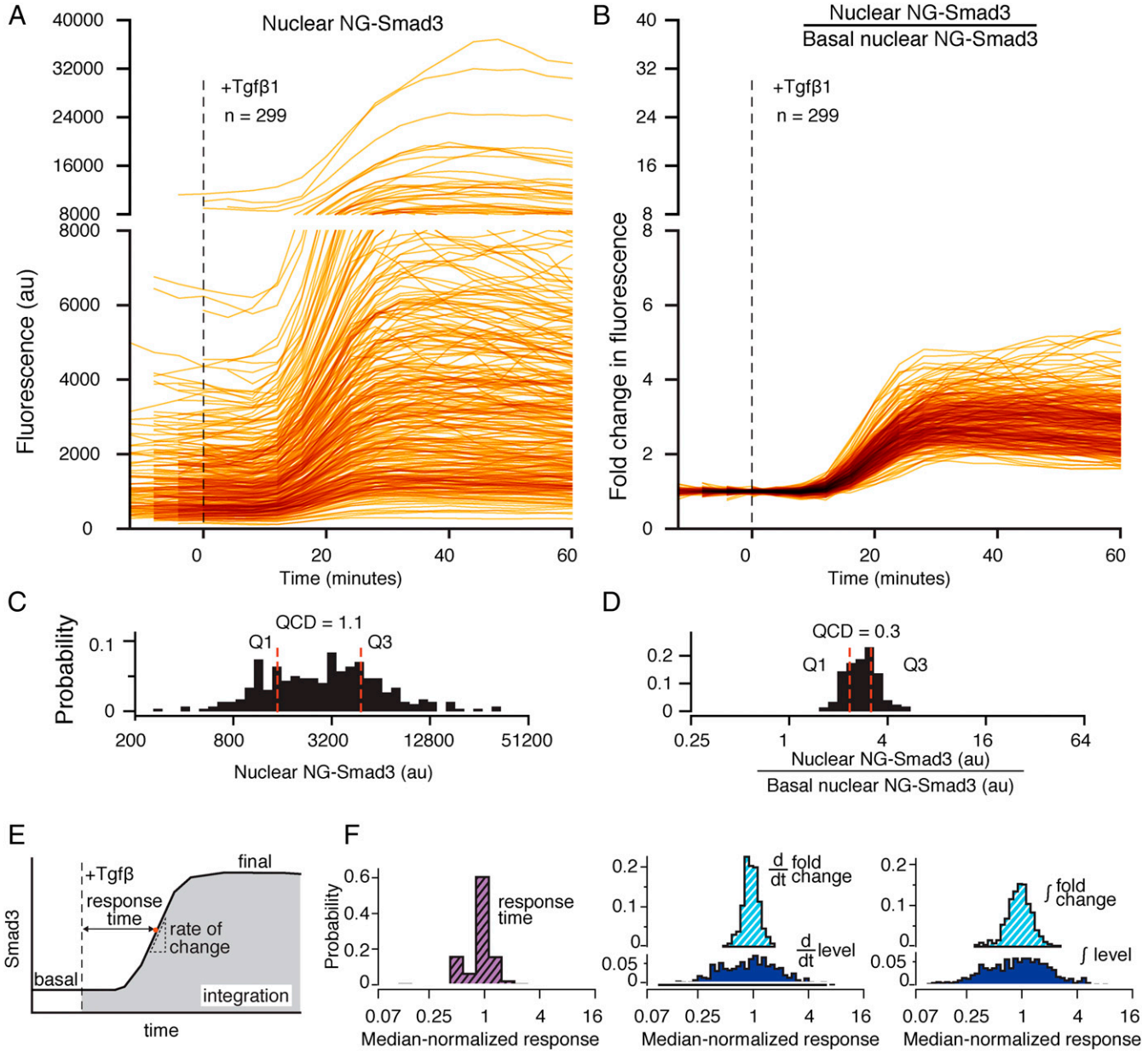

Fig. 2. Fold change in nuclear NG-Smad3 is a more precise response to ligand stimulation. (*A* and *B*) NG-Smad3 responding to 2.4 ng/mL Tgf-β1 stimulation. The dashed line indicates when Tgf-β1 was added. Each line is a trace from a single cell, plotted as the absolute fluorescence level (*A*) or relative to its basal level (*B*). Basal level was computed as the average of nuclear NG-Smad3 fluorescence in the cell over 24 min before ligand stimulation. These data came from multiple experiments. The fluorescence distribution from each experiment was adjusted so that the median fluorescence is equal across experiments. No systematic differences were observed across experiments (Fig. S3). Distribution of the level (*C*) and fold change in the level (*D*) of nuclear NG-Smad3 at 32 min after ligand stimulation are shown. Quartile coefficient of dispersion (QCD) is defined here as: (Q3 − Q1)/Q2, where Q1, Q2, and Q3 are the 25th, 50th, and 75th percentiles, respectively. (*E*) Illustration of the different response features examined in *F*. Response time was computed as the time from ligand addition until the inflection point in the response curve. Rate of change was computed as the maximum derivative of the response curve. Integrated response was computed over 52 min after ligand stimulation. (*F*) Distributions of the response time (purple), maximum rate of change, and integrated response computed from the absolute level (light blue) or fold change in nuclear NG-Smad3 (dark blue). The distributions are median-normalized to facilitate comparison. The distribution for response time is the same for fold change and absolute level, because it is defined as the time to maximum rate of change (the inflection point). Thus, only one distribution is shown.

Two features of the fold-change response are notable. First, the higher precision of the fold-change response persists throughout the duration of signaling, and not only at steady state (Fig. S5*A*). Further, the response time of the fold-change response is well preserved across cells (purple-hatched distribution in Fig. 2*F*). As a result, multiple features of the fold-change response are also more precise than the corresponding features computed using the absolute response, specifically, any monotonic functions, such as the integrated amount or the rate of change (Fig. 2 *E* and *F*). Cells therefore may derive multiple robust computations from the Smad3 response sensed relative to background (e.g., integration, rate detection, timer).

The higher precision of the fold-change response suggests that cells could better sense external ligand by monitoring Smad3 response relative to background. To assess this possibility, we collected dose–response data, which we then analyzed using information theory. First, to test if the precision of the fold-change response is maintained at different doses of ligand, we stimulated

cells with Tgf-β1 concentrations between 10 pg/mL and 2.4 ng/mL (which spans the dynamic range in our system). We observed that the fold change of NG-Smad3 increased as the dose of ligand stimulation increased, and remained a more precise response across ligand doses (Fig. 3). Correspondingly, monotonic functions of the fold-change response (e.g., integration, derivative) also maintained precision across ligand doses and display dose dependence.

Next, we analyzed the dose–response data using information theory. Pioneered by Claude Shannon in telecommunication (19), information theory provides a mathematical framework for assessing information transmission across a communication channel, whether it be an electronic device (e.g., telegraph) or a signal transduction pathway (1, 4–6, 20). Specifically, the metric mutual information describes the extent to which measuring a particular response reduces uncertainty about the input (detailed in *Materials and Methods*). Because of noise in the communication channel, a given input will not necessarily produce a given response, but rather maps to a distribution of possible responses. The greater the noise, the greater the overlap is in the response distributions, and the lower the information is that the response gives about the input (Fig. 4*A*).

To assess how the fold-change response facilitates information transduction in the Tgf-β pathway, we computed the maximum mutual information in the system. This quantity, also known as the channel capacity, describes the maximum amount of transducible information for a given input–response pair, and can be computed from measured dose–response distributions without making assumptions about the statistical properties of the input, the specifics of the transduction process, or the noise properties. Using the single-cell dose–response data in Fig. 3, we first determined the maximum mutual information between the level of nuclear NG-Smad3 and Tgf-β input (*Materials and Methods*). The level of nuclear NG-Smad3 produced overlapping distributions across Tgf-β doses (Fig. 4*B*), and could transduce, at most, ∼0.2 bits of information (Fig. 4*D*). The fold change of NG-Smad3, in contrast, produced considerably less overlap across Tgf-β doses (Fig. 4*C*), and could transduce 1.2 bits of information (Fig. 4*D*). Importantly, sensing fold change provides more information than absolute level throughout the entire signaling dynamics, even after only 8 min after ligand stimulation (Fig. S5*B*). We extended the analysis to multiple computations from the Smad3 response (e.g., integration, rate of change), and found that relative computations consistently transduce higher information than what their absolute counterparts could transduce (Fig. 4*D*). Therefore, as expected from the higher precision across cells, our results suggest that information about the Tgf-β input is more accurately transmitted through the fold change in nuclear NG-Smad3.

The robustness of and the higher information carried by the fold-change response raise the question of whether target genes use this feature and respond to the fold change in nuclear Smad3. To test this possibility, we combined live-cell imaging with single-molecule RNA FISH (Fig. 5*A*). By keeping track of the position of the cells within the imaging field, we could measure the NG-Smad3 response, and subsequently obtain mRNA counts from the same cell. We can, therefore, correlate, within single cells, both the signaling dynamics and target gene expression (3, 21). We first filmed cells responding to Tgf-β1 stimulation, and then fixed cells and stained for mRNA. To count the mRNA molecules, we took optical z-sections of the entire cells and performed automated detection of mRNA foci using custom MATLAB scripts (*Materials and Methods*).

We examined known direct targets of Smad3, *snail*, and *ctgf*. Smad3 has been shown to bind directly to the promoters of these genes upon Tgf-β stimulation (22, 23). Both genes are involved in various processes, including epithelial-mesenchymal transition, cell adhesion, fibrosis, and extracellular matrix remodeling (24, 25). For each gene, we characterized the expression profile over 6 h and report here the transcript counts at peak expression, which occurs at 1 h after ligand stimulation.

We observed variability in the mRNA expression of the target genes, which may be due to variability in cell size, chromatin state, cell-cycle phase, other extrinsic variables, or stochastic noise. Although many factors can contribute to gene regulation, we focus here on discerning the effects of Smad3 dynamics. While the variability may mask some of the correlation, clear trends were observable (Fig. 5). The expression of both target genes appeared to be linearly proportional to the magnitude of fold change in Smad3 level and showed no strong dependence on the absolute level of Smad3. Fig. 5 shows the mRNA counts plotted against the absolute level (Fig. 5*B*, *Left*) or the fold

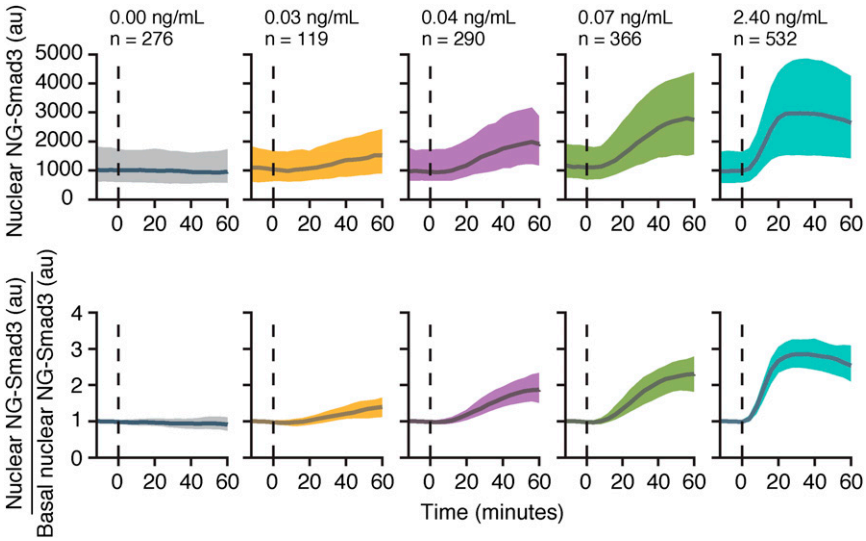

Fig. 3. Higher precision of fold-change response holds across doses of Tgf-β. Plotted is the median (bold line) bounded by the 25th percentile and 75th percentile of the data (shaded area) from traces of the level of nuclear NG-Smad3 (*Upper*) and the fold change of nuclear NG-Smad3 (*Lower*). The dashed line indicates the time of Tgf-β addition.

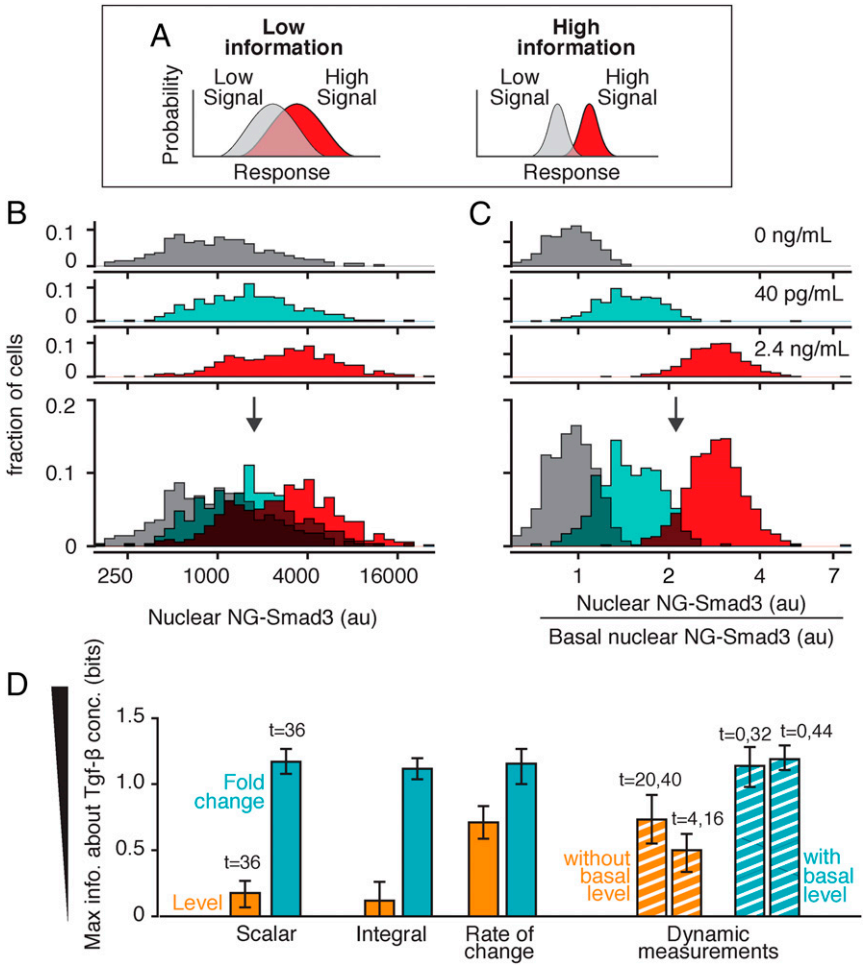

Fig. 4. Fold-change response has higher information transduction capacity. (*A*) Noisy, overlapping response distributions provide low information about the strength of ligand input. (*B* and *C*) To compute the maximum mutual information, we stimulated the cells with different doses of Tgf-β1 (Fig. 3). The response distributions for three doses are shown here, of the absolute fluorescence level (*B*) or the fold change (*C*). (*Bottom*) Overlay of the distributions. For low, medium, and high doses, the number of cells examined was 277, 290, and 532, respectively. (*D*) We computed the maximum mutual information between ligand input and different features of the nuclear NG-Smad3 response. Features computed using the absolute response are shown in orange, and features computed using the fold-change response are shown in blue. Level and fold change of nuclear NG-Smad3 were evaluated at steady state, at 36 min after Tgf-β addition (comparison at different time points is shown in Fig. S5*B*). Rate of change in the NG-Smad3 response was computed as the maximum of the derivative of the response curve. To compute the integral of the NG-Smad3 response, the response was integrated over the first hour of ligand stimulation. For dynamic measurements, the level of nuclear NG-Smad3 was measured at multiple time points, as indicated, and mutual information was computed with a 2D distribution (Fig. S8). Error bars are 90% confidence intervals computed using bootstrap resampling. The total number of cells examined for each calculation was 1,650.

change in the level of nuclear NG-Smad3 (Fig. 5*B*, *Right*). Further, the higher correlation of mRNA expression and the fold-change response was apparent throughout the entire duration of NG-Smad3 dynamics (Fig. 5*C*), and was statistically significant ($P < 0.01$, Steiger's Z test; Table S1). The same result was observed with another direct target gene, *wnt9* (Fig. S6). These results suggest that some target genes of the Tgf-β pathway respond to the fold change in Smad3, rather than the absolute level.

Discussion

There has been growing evidence that the dynamics of Smad proteins are important for their functioning (11, 18). In this study, we explored the dynamics of R-Smads to investigate how the Tgf-β pathway solves the problem of cellular variability. First, using single-cell live imaging, we found that fold change in Smad3 level, rather than absolute level, is the outcome of ligand stimulation that is more robust to cell-to-cell variation. Then, analyzing the response distributions across doses, we found that measuring fold change in Smad3 indeed confers higher information transduction capacity to the Tgf-β pathway. The robustness and higher information transduction capacity suggest that fold change in Smad3 is a meaningful signal sensed by the cells. Measuring gene response and Smad3 dynamics in single cells, we found that some direct targets of Tgf-β indeed correlate more strongly with fold change in Smad3, rather than absolute level. Altogether, these findings suggest that, at least in some contexts, cells sense the relative level of Smad3 as a way to transmit information more accurately despite cellular variability (Fig. 6).

Sensing the relative change in Smad3 may be useful for allowing the Tgf-β pathway to function reliably in diverse processes (e.g., migration, differentiation, cell death) and diverse tissues (e.g., adipose, muscle, epithelia) (10), where concentrations of the components of the pathway are known to vary significantly across cells (12), tissues (26), and developmental stages (26). The finding that signal may be sensed relative to background also means that a high level of nuclear Smad complex does not necessarily indicate a high level of signaling, and this finding may have implications for understanding the context-dependent outcomes of

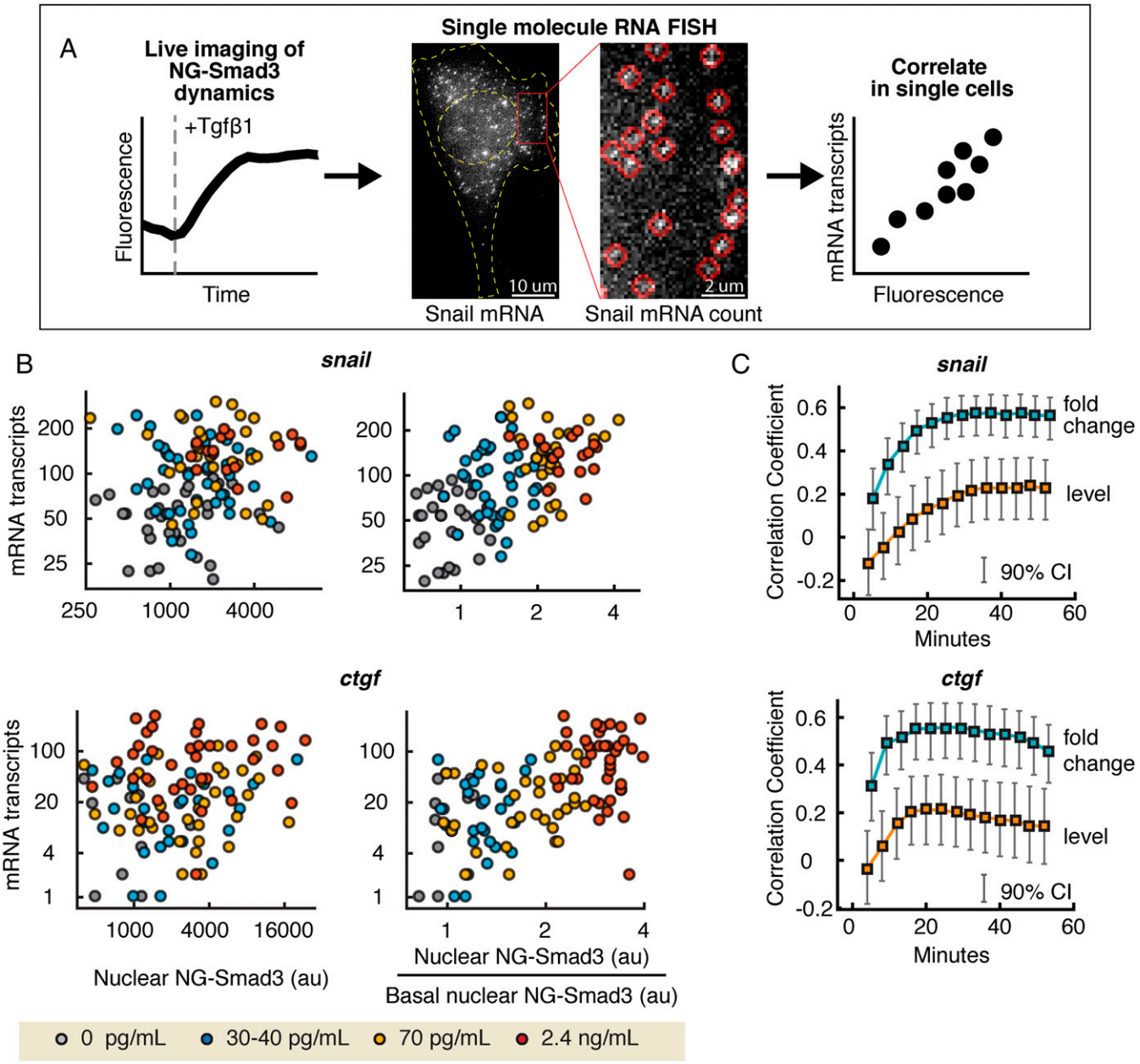

Fig. 5. Expression of target genes correlates more strongly with the fold change in nuclear NG-Smad3. (*A*) To correlate NG-Smad3 dynamics and transcription response within a single cell, we combined live-cell imaging with smFISH. Cells were stimulated with Tgf-β1 and imaged. The same cells were then fixed, stained against specific mRNA, and imaged again. Foci corresponding to individual mRNA molecules were quantified using custom MATLAB scripts. The mRNA transcript counts were then plotted against features of NG-Smad3 response from the same cells. (*B*) Number of mRNA transcripts plotted against the level (*Left*) or fold change (*Right*) of nuclear NG-Smad3 measured in the same cell. The mRNA transcripts were counted after 1 h of Tgf-β stimulation, and plotted here with response features measured at 44 min (*snail*) and 28 min (*ctgf*) after ligand stimulation. (*C*) Plotted is the correlation between mRNA transcripts (at 1 h after ligand stimulation) and NG-Smad3 response measured throughout the entire signaling dynamics. The correlation coefficient is Spearman's rank correlation coefficient. Error bars are 90% confidence intervals (CI), computed using bootstrap resampling. At each time point after ligand addition, the correlation with fold change (blue) is significantly higher than the correlation with level (orange) ($P < 0.01$, Steiger's Z test; a complete statistical analysis is shown in Table S1).

the Tgf-β pathway. For instance, the Tgf-β pathway is known to act as a tumor suppressor in early tumorigenesis and as a tumor promoter in the later stages (27). This and other context-dependent outcomes are thought to arise from cell type-specific interactions between Smads and master transcription factors, the epigenetic status of target gene promoters/enhancers, and cross-talk with other pathways (10, 28). In the framework of fold-change detection, a part of the context-dependent outcomes may arise from the signal being interpreted relative to different quantitative backgrounds.

The higher precision of the fold-change response is predicted by mathematical modeling of the Tgf-β pathway. A mathematical model capturing the nucleocytoplasmic dynamics of Smads upon Tgf-β stimulation was developed by Schmierer et al. (11). The model displays a high degree of predictive power, fitting four independent measurements in cells and predicting results from two independent datasets that were not used to construct the model. We find that simulations of the Tgf-β model predict that fold change in nuclear Smad3 will be more robust to parameter

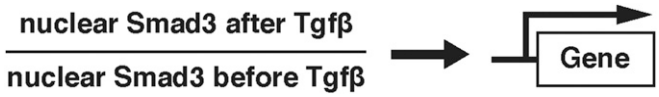

Fig. 6. Our finding suggests that, at least in some contexts, Smad signal in the Tgf-β pathway is sensed in a relative manner.

variation than the absolute level of nuclear Smad3 (Fig. S7). The robustness also holds and is even more pronounced for the fold change in the Smad complex. The parameter sensitivity analysis also indicates that the robustness in the fold-change response starts breaking down with large-parameter variations, indicating that cells must operate in a specific parameter regime to achieve this robust feature in Smad3 response (Fig. S7 *C* and *D*). Similar parameter tuning is also required in the fold-change response in the canonical Wnt pathway (7). Overall, these results suggest that the robust fold-change response arises from the conserved interactions of the pathway.

The higher precision of the fold-change response of Smad3 significantly increases the information transduction capacity of the Tgf-β pathway. It was recently proposed that measuring the absolute signal dynamics over multiple time points may increase channel capacity in Erk, NF-κB, and the calcium pathway (6). We tested this idea in the Tgf-β pathway and found that measuring the signaling dynamics of Smad3 at multiple time points can give comparable mutual information to the fold-change response, provided that one of the time points was the basal state (Fig. 4*D* and Fig. S8), therefore strengthening our findings here. Our findings suggest that, despite variability in the Smad level, there is indeed reliable signal processing within the Tgf-β pathway.

Looking downstream in the pathway, the correlation between target gene expression and fold change in Smad3 necessitates a mechanism for computing fold changes. A recurrent motif in transcriptional networks, the type-1 incoherent feedforward loop, was shown to have the ability to provide fold-change computation (29). Smads, known activators, also effect repression through recruitment of repressors, such as ATF3 or E2F4 (30), or inducing specific microRNAs that repress their own target genes (31). In the context of our findings, these seemingly opposite actions of Smads may mediate fold-change detection.

Our present work places the Tgf-β pathway among the increasing number of signaling pathways where fold-change response has now been identified or proposed (2, 3, 7–9). Our finding reinforces an emerging theme across signaling pathways in animal cells, that signaling dynamics are sensed in a relative manner. Beyond signaling in cells, sensing signal in a relative manner brings to mind the Weber's law in sensory systems (32–34), and highlights a convergence between biological sensory systems at the single-cell and organismal levels.

Materials and Methods

Expression Construct. The human Smad3 cDNA was a gift from Joan Massague (Addgene; plasmid 27010). Human Smad3 and mouse Smad3 contain 100% sequence identity. The mNeonGreen (NG) gene was obtained from Allele Biotechnology (ABP-FP-MNEONSA). The mCerulean3-C1 cDNA was a gift from Klaus Hahn (Addgene; plasmid 22030). The NG-Smad3 construct was placed downstream of a CMV promoter, and the mCerulean3 gene was fused with a 3× nuclear localization sequence (NLS) and placed downstream of an SV40 promoter.

Cell Culture. C2C12 cells (American Type Culture Collection, CRL-1772) were cultured at 37 °C and 5% (vol/vol) CO_2 in DMEM (ThermoFisher Scientific; 11995) supplemented with 10% (vol/vol) FBS (Invitrogen; A13622DJ), 100 U/mL penicillin, 100 μg/mL streptomycin, 0.25 μg/mL amphotericin, and 2 mM L-glutamine (Invitrogen). To generate the NG-Smad3 C2C12 cell line, cells were transfected with the NG-Smad3 plasmid using FuGene 6 reagent (Promega; E2693). Stable expression was selected for using puromycin at a concentration of 2 μg/mL. Cells were sorted using FACS and then plated in a 96-well plate to select single clones. NG-Smad3 cells were maintained in media containing 2 μg/mL puromycin.

Live-Cell Imaging. Cells were grown on 24-well glass-bottomed plates (Griener Bio-One; 662892) overnight before imaging in 2 mL of FluoroBrite DMEM (Gibco-Life Technologies; A18967) containing 10% (vol/vol) FBS, 1 mM glutamax (Gibco-Life Technologies; 35050), 1 mM sodium pyruvate, 100 U/mL penicillin, 100 μg/mL streptomycin, and 0.25 μg/mL amphotericin. Cells were imaged using a Zeiss Axio Observer.Z1 inverted fluorescence microscope under incubation [37 °C and 5% (vol/vol) CO_2, with humidification] on a motorized stage. In each experiment, 21–38 positions were imaged and focus was maintained using Zeiss Definite Focus. Images were acquired at 4-min intervals with a 20×, 0.8-N.A. Plan Apo objective and Evolve 512 EM-CCD camera (Photometrics). Cells were imaged for at least 1 h before stimulation with Tgf-β1 (PeproTech; 100-21). One hundred microliters of Tgf-β–containing media was added to cells to achieve desired final concentrations of Tgf-β in cell growth media for experiments. Buffer-only media were added in 0 ng/mL experiments to control for any effects of adding liquid (e.g., shear stimulation).

Image Analysis, Cell Tracking, and Fluorescence Quantification. Time-lapse movies were quantified after flat-field correction, bleaching correction, and background subtraction. We followed the standard protocol described by Waters (35). In flat-field correction, to capture the shape of fluorescence illumination, we imaged a well containing media only. We imaged five different positions within the well, and computed the median of the images. Flat-field correction was performed by dividing each experimental image by this media-only image. This procedure was repeated for each fluorescence channel. Bleaching correction was performed for each fluorescence channel by correcting for the global change in fluorescence throughout the duration of imaging. For background correction, images were segmented such that the entireties of cells were broadly outlined, and fluorescence signal from the background was then averaged and subtracted from the image. This procedure was repeated for all images at each time frame.

Fluorescence Quantification. We report the median fluorescence intensity of NG-Smad3 fluorescence in the nuclei. The nuclei of cells were first segmented based on the fluorescence of the constitutively expressed mCerulean3-3NLS (3×NLS). Next, segmented nuclei were tracked across all time frames. Finally, the fluorescence data from the segmented nuclei were extracted. We only tracked and quantified fluorescence from cells that maintained consistent morphology for at least 1 h of imaging. Cells that divided, balled up, left the imaging field of view, or displayed some abnormality (e.g., double-nucleated, abnormally large) were excluded.

For correcting experimental fluctuations during the imaging period, we used the constitutive mCerulean3 fluorescence as an internal control, dividing each time trace for NG-Smad3 nuclear fluorescence by the normalized mCerulean fluorescence time trace in the same cell. Subsequently, individual time traces were smoothed using a running three-frame average. mCerulean normalization and time trace averaging turn out to be minor corrections (likely because our tracked cells maintained consistent morphology and our imaging setup was stable during imaging duration), and we obtained the same conclusions both with and without these corrections applied (raw data are available upon request).

We performed all segmentation, tracking, and fluorescence quantitation steps using the Lineage Tracker ImageJ (NIH) plug-in (36) and custom MATLAB (MathWorks) scripts (available upon request).

Single-Molecule FISH. Following time-lapse imaging, cells were fixed using 4% (wt/vol) paraformaldehyde for 20 min, permeabilized in 70% (vol/vol) ethanol for at least 1 d at −20 °C, and then hybridized overnight with HPLC-purified single-molecule FISH (smFISH) probes at 30 °C using a protocol adapted from Raj et al. (37). Images of stained cells were acquired using a 40×, 1.4-N.A. Plan Apo Oil Objective with Immersol 518F (Zeiss; 444960) and an Orca Flash 4.0 V sCMOS camera. To ensure the entirety of each cell was imaged at each position, a z-stack of 20 or more images was collected at 0.6-μm intervals. Differential interference contrast (DIC) images from the middle Z-slice of image stacks were used for manual segmentation of cells. The mRNA foci were detected using custom MATLAB scripts. Briefly, fluorescence images were convolved with a 5 × 5 Laplacian-of-Gaussian kernel, and then thresholded such that mRNA foci were only identified in cells (scripts available upon request). Probe sets targeting *snai1*, *wnt9a*, and *ctgf* mRNA were designed using Stellaris Probe Designer Version 4.1 and ordered from Biosearch. Each probe is a 20-mer with a mdC(TEG-Amino) 3′ modification, which was used to couple the probe to Alexa Fluor 594 NHS Ester (Molecular

Probes; A20004) or Alexa Fluor 647 NHS Ester (Molecular Probes; A20006). Following the coupling reaction, fluorescently labeled probes were purified using HPLC. The smFISH probe sequences are provided in Table S2.

Mutual Information Estimation. To estimate the mutual information between Tgf-β input and NG-Smad3 response, we followed the steps described in the methods of Voliotis et al. (5). Mutual information is expressed as follows:

$$I(R;S) = h(R) - h(R|S) = h(R) - E[h(R|S=s)], \quad [1]$$

where R, the pathway output, is continuous and possibly multivariate, and S, the ligand input, is the distribution of ligand concentrations. R is a vector containing experimentally determined responses (e.g., a vector of fold-change responses at $t = 32$ min or a vector of nuclear NG-Smad3 levels at $t = 32$ min), and S is a vector containing the probabilities of ligand doses.

The unconditional entropy, $h(R)$, and the conditional entropy, $h(R|S=s)$, are estimated using the nearest-neighbor (knn) method [i.e., equation 20 of Kraskov et al. (38)], which is reproduced below:

$$\hat{H}(X) = -\psi(k) + \psi(N) + \log c_d + \frac{d}{N}\sum_{i=1}^{N} \log \varepsilon(i). \quad [2]$$

The knn method performs better than "binning with bias correction" (used in ref. 1), at a smaller sample size ($n < 200$), giving more accurate estimations of mutual information with smaller mean squared error and bias (5). We use $k = 3$ nearest neighbors for all estimations performed in this work.

For each calculation of mutual information, we performed 100 iterations of random sampling (without replacement) of the dataset. We confirmed that the distributions of the mutual information estimator are similar for 100 and 1,000 iterations. To determine maximum mutual information, we tested 100 different signal input distributions, S, ranging from uniform, to unimodal, to bimodal, to trimodal, and determined the signal at which mutual information was maximum. We report in Fig. 4*D* and Fig. S8 the maximum mutual information. To compute the mutual information using dynamic measurement (6), R is multivariate, with each entry in R (corresponding to a single cell) containing two time point measurements.

ACKNOWLEDGMENTS. We thank Michael Abrams, Zakary Singer, and Kibeom Kim for insightful comments on the manuscript. We also thank Xun Wang for sharing plasmid constructs, Yaron Antebi for help in developing cell tracking and segmentation scripts, and especially, Zakary Singer, Eric Lubeck, and Long Cai for help with smFISH. We thank Diana Perez and Rochelle Diamond (Caltech Flow Cytometry and Cell Sorting Facility) for expert cell sorting. We thank Eric Batchelor and Michael Elowitz for discussions on the study. This work was supported by NIH Training Grants 2T32GM007616-36 (to C.L.F.) and 5T32GM007616-37 (to H.N.), NIH New Innovator Award DP2OD008471, the James S. McDonnell Scholar Award in Complex Systems (Grant 220020365), and National Science Foundation Career Award NSF.1453863 (to L.G.).

1. Cheong R, Rhee A, Wang CJ, Nemenman I, Levchenko A (2011) Information transduction capacity of noisy biochemical signaling networks. *Science* 334(6054):354–358.
2. Cohen-Saidon C, Cohen AA, Sigal A, Liron Y, Alon U (2009) Dynamics and variability of ERK2 response to EGF in individual living cells. *Mol Cell* 36(5):885–893.
3. Lee RE, Walker SR, Savery K, Frank DA, Gaudet S (2014) Fold change of nuclear NF-κB determines TNF-induced transcription in single cells. *Mol Cell* 53(6):867–879.
4. Uda S, et al. (2013) Robustness and compensation of information transmission of signaling pathways. *Science* 341(6145):558–561.
5. Voliotis M, Perrett RM, McWilliams C, McArdle CA, Bowsher CG (2014) Information transfer by leaky, heterogeneous, protein kinase signaling systems. *Proc Natl Acad Sci USA* 111(3):E326–E333.
6. Selimkhanov J, et al. (2014) Systems biology. Accurate information transmission through dynamic biochemical signaling networks. *Science* 346(6215):1370–1373.
7. Goentoro L, Kirschner MW (2009) Evidence that fold-change, and not absolute level, of β-catenin dictates Wnt signaling. *Mol Cell* 36(5):872–884.
8. Thurley K, et al. (2014) Reliable encoding of stimulus intensities within random sequences of intracellular Ca2+ spikes. *Sci Signal* 7(331):ra59.
9. Thurley K, Gerecht D, Friedmann E, Höfer T (2015) Three-dimensional gradients of cytokine signaling between T cells. *PLOS Comput Biol* 11(4):e1004206.
10. Massagué J (2012) TGFβ signalling in context. *Nat Rev Mol Cell Biol* 13(10):616–630.
11. Schmierer B, Tournier AL, Bates PA, Hill CS (2008) Mathematical modeling identifies Smad nucleocytoplasmic shuttling as a dynamic signal-interpreting system. *Proc Natl Acad Sci USA* 105(18):6608–6613.
12. Zieba A, et al. (2012) Intercellular variation in signaling through the TGF-β pathway and its relation to cell density and cell cycle phase. *Mol Cell Proteomics* 11(7):013482.
13. Brown KA, Pietenpol JA, Moses HL (2007) A tale of two proteins: Differential roles and regulation of Smad2 and Smad3 in TGF-beta signaling. *J Cell Biochem* 101(1): 9–33.
14. Gaarenstroom T, Hill CS (2014) TGF-β signaling to chromatin: How Smads regulate transcription during self-renewal and differentiation. *Semin Cell Dev Biol* 32:107–118.
15. Nicolás FJ, De Bosscher K, Schmierer B, Hill CS (2004) Analysis of Smad nucleocytoplasmic shuttling in living cells. *J Cell Sci* 117(Pt 18):4113–4125.
16. Baker JC, Harland RM (1996) A novel mesoderm inducer, Madr2, functions in the activin signal transduction pathway. *Genes Dev* 10(15):1880–1889.
17. Macías-Silva M, et al. (1996) MADR2 is a substrate of the TGFbeta receptor and its phosphorylation is required for nuclear accumulation and signaling. *Cell* 87(7): 1215–1224.
18. Warmflash A, et al. (2012) Dynamics of TGF-β signaling reveal adaptive and pulsatile behaviors reflected in the nuclear localization of transcription factor Smad4. *Proc Natl Acad Sci USA* 109(28):E1947–E1956.
19. Shannon CE (1948) A mathematical theory of communication. *Bell System Technical Journal* 27(3):379–423.
20. Hansen AS, O'Shea EK (2015) Limits on information transduction through amplitude and frequency regulation of transcription factor activity. *eLife* 4:e06559.
21. Singer ZS, et al. (2014) Dynamic heterogeneity and DNA methylation in embryonic stem cells. *Mol Cell* 55(2):319–331.
22. Brandl M, et al. (2010) IKK(α) controls canonical TGF(ß)-SMAD signaling to regulate genes expressing SNAIL and SLUG during EMT in panc1 cells. *J Cell Sci* 123(Pt 24): 4231–4239.
23. Zhang Y, et al. (2011) High throughput determination of TGFβ1/SMAD3 targets in A549 lung epithelial cells. *PLoS One* 6(5):e20319.
24. Fan W-H, Pech M, Karnovsky MJ (2000) Connective tissue growth factor (CTGF) stimulates vascular smooth muscle cell growth and migration in vitro. *Eur J Cell Biol* 79(12):915–923.
25. Medici D, Hay ED, Olsen BR (2008) Snail and Slug promote epithelial-mesenchymal transition through β-catenin-T-cell factor-4-dependent expression of transforming growth factor-β3. *Mol Biol Cell* 19(11):4875–4887.
26. Flanders KC, Kim ES, Roberts AB (2001) Immunohistochemical expression of Smads 1-6 in the 15-day gestation mouse embryo: Signaling by BMPs and TGF-betas. *Dev Dyn* 220(2):141–154.
27. Akhurst RJ, Hata A (2012) Targeting the TGFβ signalling pathway in disease. *Nat Rev Drug Discov* 11(10):790–811.
28. Akhurst RJ, Padgett RW (2015) Matters of context guide future research in TGFβ superfamily signaling. *Sci Signal* 8(399):re10.
29. Goentoro L, Shoval O, Kirschner MW, Alon U (2009) The incoherent feedforward loop can provide fold-change detection in gene regulation. *Mol Cell* 36(5):894–899.
30. Massagué J, Seoane J, Wotton D (2005) Smad transcription factors. *Genes Dev* 19(23): 2783–2810.
31. Butz H, Rácz K, Hunyady L, Patócs A (2012) Crosstalk between TGF-β signaling and the microRNA machinery. *Trends Pharmacol Sci* 33(7):382–393.
32. Laming D (1986) *Sensory Analysis* (Academic, London).
33. Shepard RN, Kilpatric DW, Cunningham JP (1975) The internal representation of numbers. *Cogn Psychol* 7(1):82–138.
34. Weber EH, Ross HE, Murray DJ (1996) *E. H. Weber on the Tactile Senses* (Erlbaum (UK) Taylor & Francis, East Sussex, UK).
35. Waters JC (2009) Accuracy and precision in quantitative fluorescence microscopy. *J Cell Biol* 185(7):1135–1148.
36. Downey MJ, et al. (2011) Extracting fluorescent reporter time courses of cell lineages from high-throughput microscopy at low temporal resolution. *PLoS One* 6(12): e27886.
37. Raj A, van den Bogaard P, Rifkin SA, van Oudenaarden A, Tyagi S (2008) Imaging individual mRNA molecules using multiple singly labeled probes. *Nat Methods* 5(10): 877–879.
38. Kraskov A, Stögbauer H, Grassberger P (2004) Estimating mutual information. *Phys Rev E Stat Nonlin Soft Matter Phys* 69(6 Pt 2):066138.
39. Steiger JH (1980) Tests for comparing elements of a correlation matrix. *Psychol Bull* 87(2):245–251.